AIAA JOURNAL
Vol. 43, No. 1, January 2005

Beam Steering and Shaping of Smart Cylindrical Antenna

V. K. Gupta*
Engineering College, Kota 324 010, India
and
P. Seshu,† K. Kurien Issac,‡ and R. K. Shevgaonkar§
Indian Institute of Technology Bombay, Mumbai 400 076, India

Shape control of parabolic cylindrical antennas and corresponding effect on radiation pattern, using piezoelectric actuators, is investigated. A narrow, 350-mm-long aperture, parabolic cylindrical antenna of Lexan® material is chosen for analysis. Antenna deformation is analyzed using an experimentally validated piezoelectric shell finite element. Radiation pattern is calculated using physical optics. Significant steering and shaping are obtained by deforming the antenna using centrally placed actuators. Using the strategy of making the phase variation at aperture as linear as possible and adjusting the phase difference between the two halves of the antenna to be an integral multiple of 2π, very good quality is achieved for the steered and shaped beams.

Nomenclature

A	=	area
d_{31}, d_{32}	=	piezoelectric strain coefficients
E	=	field Intensity
$f(x)$	=	phase distribution
h	=	aperture length
k	=	phase slope
$p(x)$	=	path difference distribution
t	=	thickness
$\{u, v, w\}$	=	linear displacements
V	=	applied voltage
$\{x, y, z\}$	=	Cartesian coordinates
Y	=	Young's modulus of elasticity
β	=	beam shift
ξ, η, ζ	=	curvilinear coordinates
ϕ	=	electric field

Subscripts

p	=	piezo actuator
s	=	substructure

I. Introduction

DISTRIBUTED piezoelectric sensors and actuators, bonded to/embedded in structures, have been explored for achieving desired shape and vibration control. The key issues in such a study include the number of sensors/actuators required, their sizes, locations, the field to be applied on each actuator, and finally the feedback control algorithm. Shape control of beams and plates has been obtained by minimizing the error between the desired shape and actual shape, using distributed piezoactuators.[1–9] Both analytical[1–4] and finite element based[5–7] models of deformation have been used. Yang and Ngoi[4] gave analytical solutions for the shape control of beams by piezoelectric actuators subjected to different boundary conditions. They showed that the piezoelectric actuators can deform a beam approximately in a quadratic or a cubic curve. Recently, Irschik[9] reviewed the literature on shape control of structures using piezoelectric actuators.

One of the application areas currently being actively pursued is shape control of antenna. The central idea is to apply suitable electric fields to the actuators placed at appropriate locations on the antenna shell structure and induce the desired deformation of the antenna structure. These deformations in turn affect the path length of rays (phase difference) and hence the resulting radiation pattern. Washington[10] proposed the use of fully covered polyvinylidene fluoride (PVDF) film for shaping and steering of antennas.

Steering refers to changing the principal direction of the antenna and is used when one wants to change the scanning area from one location to another location (Fig. 1). Shaping refers to changing the area covered around the principal direction and is used when the area covered at a particular location is to be increased or decreased. Beam shaping is a broader term and can be used to refer to other ways of affecting the beam shape, for example, splitting of principal beam into a pair of symmetric beams.

Yoon and Washington[11] used PZT strips, which do not extend the full surface of the antenna. Recently, Yoon et al.[12] used piezoelectric actuators to control the spherical (doubly curved) antenna's coverage area. They applied Reisner's shell theory to derive the equations, and deformation of reflector surface was calculated analytically. In addition to reflector antennas, piezoactuation has been investigated for microstrip antennas[13] and D-fiber antennas.[14]

In the current study, piezoactuated steering and shaping of radiation of parabolic cylindrical antenna has been investigated. Deformation of antenna is calculated using shell finite elements adapted for modeling surface bonded piezoelectric actuators.[15] Radiation pattern is calculated using physical optics.[16] The aim of the study is to obtain significant steering and shaping with good radiation quality.

II. Radiation Pattern of Undeformed Cylindrical Antenna

Radiation pattern of an antenna refers to the spatial distribution of radiated energy. Physical optics (theory of diffraction) has been used here for determination of radiation pattern, which is applicable only in cases where the aperture is very large compared to wavelength. For the antennas considered in the current study, aperture size is about 350 mm and wavelength is 1 mm.

Two rays emanating simultaneously from secondary sources x distance apart on the aperture plane and traveling in direction θ would arrive at a point P at infinity, at different times as they travel different distances (Fig. 2b).

Received 1 March 2004; revision received 30 June 2004; accepted for publication 1 July 2004.

*Senior Lecturer, Mechanical Engineering Department, Engineering College Kota, Akelgarh; guptavkr@sify.com.
†Associate Professor, Mechanical Engineering Department, Powai; seshu@me.iitb.ac.in.
‡Associate Professor, Mechanical Engineering Department, Powai; kurien@me.iitb.ac.in.
§Professor, Electrical Engineering Department, Powai; rks@ee.iitb.ac.in.

Let the phase difference between the secondary source at S and at the center O be $f(x)$. The field intensity of the wave from S in direction θ is given by[17]

$$E_\theta(x) = A\,\mathrm{d}x \exp\{-j[f(x) + 2\pi(x \sin\theta/\lambda)]\} \tag{1}$$

where A is the field amplitude of the secondary sources per unit length of aperture and λ is the antenna wavelength.

Here, it is assumed that the field amplitude is uniform over the aperture. $E_\theta(x)$ is expressed as a phasor, so that the sum of field intensities from all secondary sources can be obtained in a convenient way. This phasor sum is

$$E_\theta = \int_{-h/2}^{h/2} A \exp\left\{-j\left[f(x) + 2\pi\frac{x\sin\theta}{\lambda}\right]\right\} \mathrm{d}x \tag{2}$$

E_θ is also a phasor/complex number, whose amplitude/modulus gives the total field intensity of radiation in the direction θ.

Equation (2), used for calculating radiation pattern, is valid for any width of the antenna provided the directions considered have $\phi = 0$ (Ref. 17). While calculating radiations in other directions, the effect of width has to be considered. In this study, radiation patterns in the directions with $\phi = 0$ only have been considered.

A code written in MATLAB® is used for the calculation of radiation pattern. Equation (2) is numerically integrated using the Gauss quadrature rule for each value of θ ranging from -10 to $+10$ deg at an interval of 0.02 deg. Calculating radiation field intensity at 0.02-deg intervals is found necessary to determine peak radiation field intensity with sufficient accuracy. A window of -10 to $+10$ deg is found sufficient to capture the important features of the intensity variation with respect to direction. A plot of radiation field intensity vs θ ($\phi = 0$) is given in Fig. 3 for an antenna covering 120 deg, with an aperture length of 0.35 m, focal length f of 0.151 m. (The parameters are illustrated in Fig. 4.) The wavelength used here is 1 mm, which is prevalent in astronomy applications. The main lobe is at $\theta = 0$ deg and of amplitude 0.35. Several small side lobes, symmetric about $\theta = 0$, are also visible.

A. Radiation Pattern Parameters

Three important parameters that indicate the quality of radiation pattern are directivity, half-power beam width, and side-lobe ratio. Directivity is the ratio of maximum value of radiation intensity to the average radiation intensity. The half-power beam width (HPBW), shown in Fig. 3, is a measure of the coverage of the main lobe. It

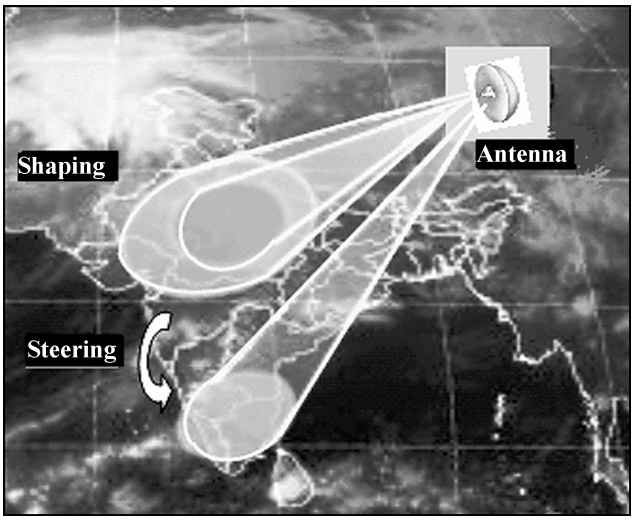

Fig. 1 Antenna shaping and steering.

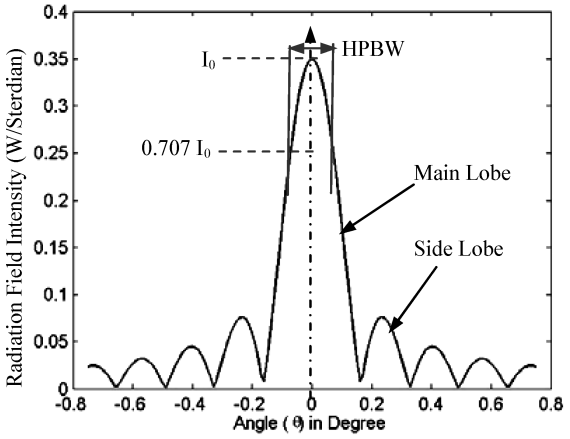

Fig. 3 Radiation pattern at $\phi = 0$ deg (uniform phase distribution).

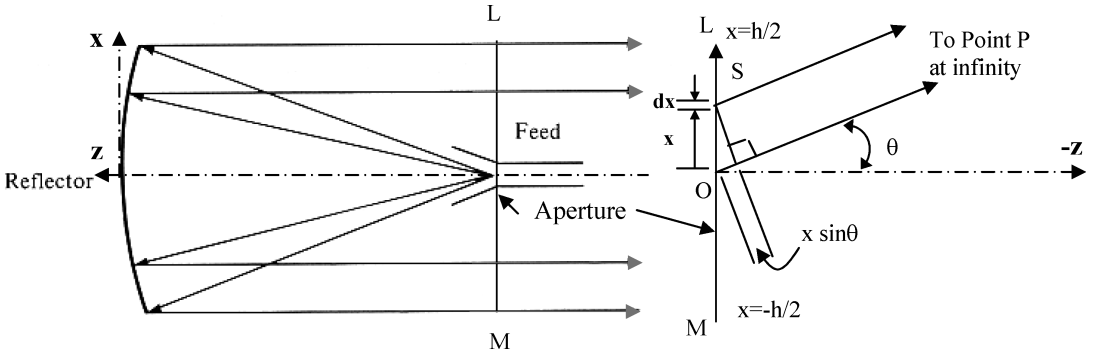

a) Parabolic reflector **b) Path traveled by a ray**

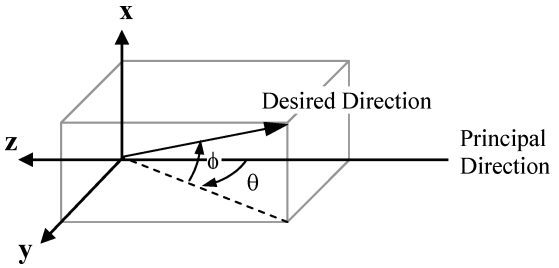

c) Direction vectors

Fig. 2 Radiation pattern calculation for parabolic reflector antenna.

is the angle between two directions in which the field intensity is 0.707 times the maximum field intensity of the main lobe. Side-lobe ratio is the ratio of the peak radiation intensity of the main lobe to the peak intensity of the side lobe.

B. Effect of Phase Variation

Phase distribution of secondary sources at aperture has significant influence on the direction of main lobe. Here effect of linear phase variation on steering of the radiation pattern is analyzed for the undeformed antenna.

If phase is linearly varied along aperture (say, phase $= kx$), the entire radiation pattern is shifted by an angle β (Fig. 5). As the slope k is increased, the main lobe shifts more. For $k = 109.95$ rad/m, the shift in main lobe, $\beta = 1$ deg, and for $k = 219.91$ rad/m, $\beta = 2$ deg. It can be shown that $\sin\beta$ is proportional to k. The shape of radiation pattern does not change significantly with the beam steering. Side-lobe levels and HPBW remain more or less the same. This effect has been used for antenna beam steering by using the feed to apply appropriate phase variation.[17]

If phase variation in the two halves is in the same direction (i.e., positive) (Fig. 6), two peaks are observed in the radiation pattern. For $k = 200$ rad/m, one peak is at -1.38 deg and another at 1.38 deg. Both peaks have amplitudes equal to half the amplitude of the peak in uniform phase variation. Side-lobe ratio remains the same as that of the uniform phase radiation while HPBW has doubled. This type of variation is useful when two noncontiguous areas are to be scanned by the antenna simultaneously.

It can be concluded that a linear variation in phase causes a shift in the main lobe, retaining the shape of the radiation pattern. Two separate radiation peaks are obtained with symmetric, piecewise linear phase variation. Nonlinear phase variations were also studied.[15] They lead to deterioration of radiation pattern quality by increasing the side-lobe intensity and the number of side lobes. Steering and shaping of the radiation pattern are now attempted by inducing linear and piecewise linear phase variations by deforming the antenna using piezoelectric actuators.

III. Use of Piezoelectric Actuators to Influence Antenna Radiation Pattern

The central idea here is to apply suitable electric fields to the actuators, placed at appropriate locations on the antenna shell structure, and induce the desired deformation of the antenna structure. These deformations, in turn, affect the path length of rays (phase difference) and hence the resulting radiation pattern. A finite element model is developed to calculate the deformations of cylindrical antenna surface under the piezoelectric actuation, details of which are described in the following section.

A. Finite Element Analysis of Antenna Deformation

Ahmad et al.'s[18] eight-noded reduced shell element (Fig. 7) is used to develop the finite element (FE) model. The FE formulation

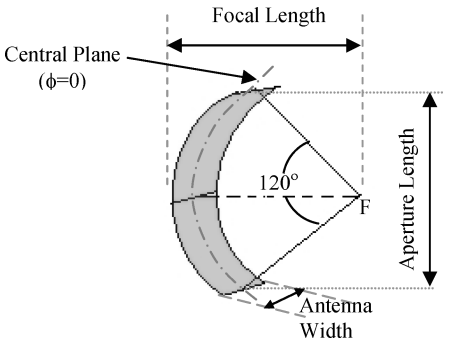

Fig. 4 Antenna dimension parameters.

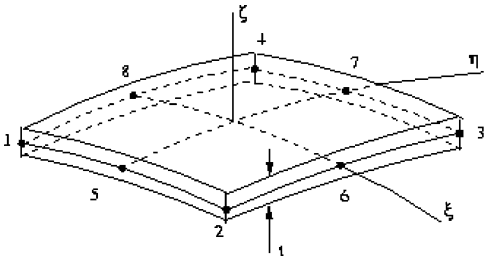

Fig. 7 Reduced shell element.[18]

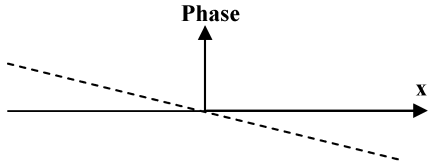

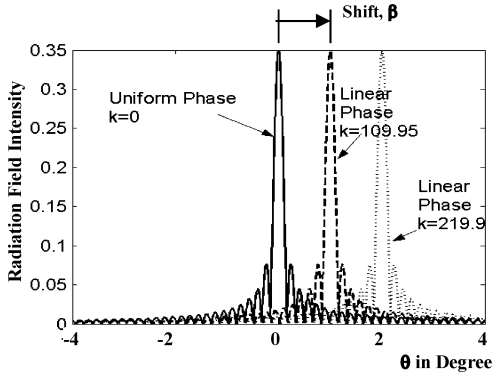

Fig. 5 Linear phase variation for steering [wavelength = 1 mm, aperture length = 0.35 m, focal length $f = 0.151$ m, angle covered $(2\alpha) = 120$ deg].

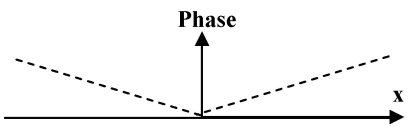

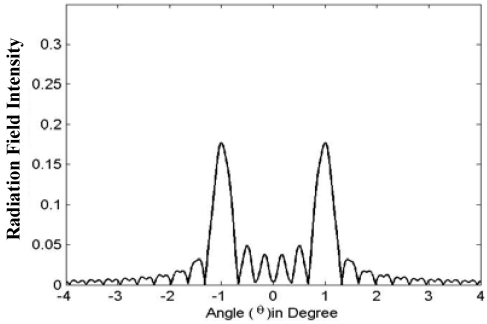

Fig. 6 Piecewise linear phase variation for shaping [wavelength = 1 mm, aperture length = 0.35 m, focal length $f = 0.151$ m, angle covered $(2\alpha) = 120$ deg].

is discussed in detail in Gupta et al.[19] Each node on the reduced shell element has five deg of freedom, three nodal displacements (u, v, w), and two rotations (α, β).

A typical piezoelectric shell element is shown in Fig. 8. It contains three layers, two piezoelectric (upper and lower) layers bonded on either side of the shell substrate layer. Material properties of piezoelectric material differ from the properties of the substructure and hence are not a continuous function of ζ. Hence the layered theory as proposed by Panda and Natarajan[20,21] is applied to consider the effect of different layers. When an electric field ($\phi = V/t_p$) is applied on piezoelectric actuator, a free piezostrain ε_{pf} will develop in the actuator. This has been modeled as initial strain problem. It is assumed that the actuator is perfectly bonded to the structure.

B. Experimental Validation

Experiments are conducted on straight and cylindrical curved beams to verify the FE formulation. A curved-beam specimen with bonded piezoelectric actuators, along with typical equipment/instruments used, is shown in Fig. 9.

An electric field is supplied to the actuator by a high-voltage (200 V) and low-current (200 mA) power amplifier. The deflection caused by piezoelectric actuation is measured using a noncontact fiber-optic displacement sensor.

The straight beam specimen and a comparison of the finite element predicted and experimentally observed response of the beam under piezoactuation are shown in Fig. 10. The fiber-optic sensor is traversed along the length of the beam and the deflection of the beam recorded. It is observed that the finite element prediction of the deflected shape matches very well with the experimental observations.

The circular curved-beam specimen used in experiment is shown in Fig. 11a and a typical finite element mesh in Fig. 11b. Effect of voltage variation on deformation of the beam is shown in Fig. 11c.

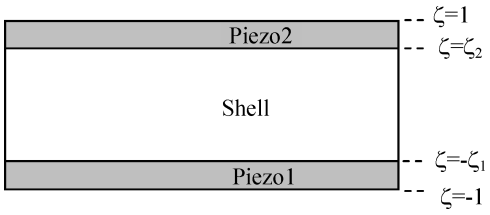

Fig. 8 Piezoelectric shell element.

Finite element method and experimental results show a maximum deviation of 25% at 88 V, but this is only 3.3% at 45 V. Experimental results indicate nonlinear behavior especially at higher voltages. Hysteresis curves have been obtained under cyclic variation of voltage.[15]

C. Antenna Deformation and Phase Variation

Effect of piezoelectric actuation on antenna performance is analyzed now. Deformations caused by piezoelectric actuation are calculated using the finite element code developed.[19] It is assumed that the antenna is rigidly fixed at the apex. For deformation calculation, 1050 elements are used in the length direction and three elements in the width direction (Fig. 11b). The material properties of the antenna considered are given in Table 1. An antenna with aperture length = 0.35 m, focal length $f = 0.151$ m, and angle covered = 120 deg (these parameters are illustrated in Fig. 4)

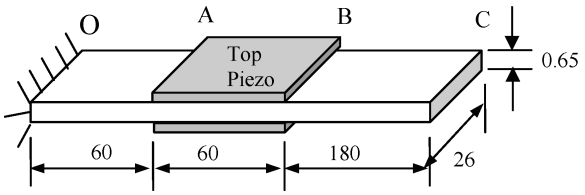

a) Dimensions (millimeters)

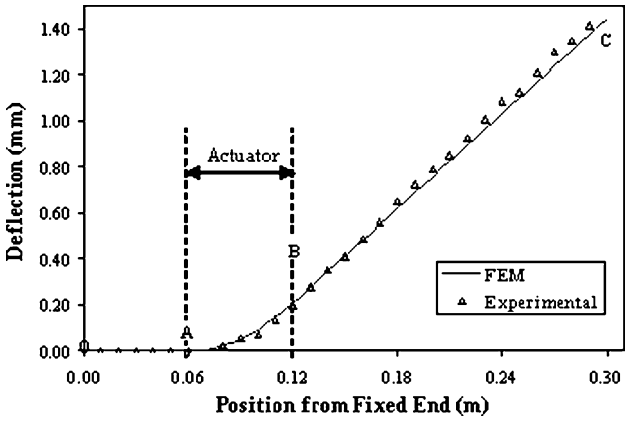

b) Deflection along the length of cantilever beam under piezoactuation

Fig. 10 Straight-beam experiments.

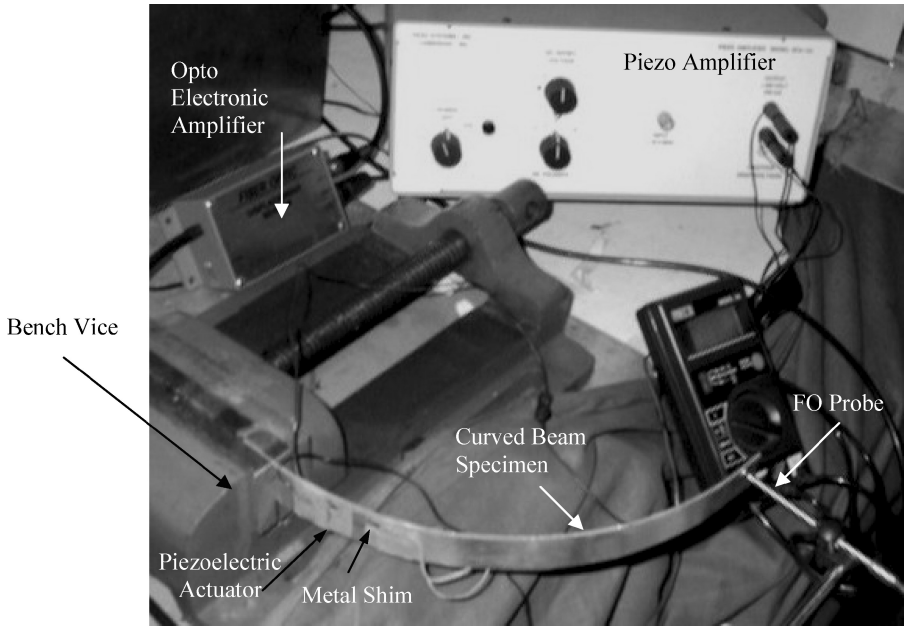

Fig. 9 Experimental setup.

is considered. The wavelength used here is 1 mm. Piezo System, Inc.'s, PSI-5A-S4-ENH[22] is used here as a piezoelectric actuator, the properties of which are summarized in Table 2.

The phase variation caused by deformation of the antenna can be calculated as follows, considering only the middle line of the antenna (line AB in Fig. 11b) and corresponding deformations. Figure 12 shows a deformed antenna with deflections exaggerated. Point N on the antenna surface, is shifted to point N′, mainly in the z direction as x and y displacements are negligible. It is assumed that the deflection of antenna is very small and the rays from focus, when reflected from the antenna shell, travel parallel to the axis of the parabola.

Table 1 Material properties of cylindrical antenna

Material	Lexan®[a] (ASTM-D3935)
Modulus of elasticity	2.3×10^9 N/m^2
Thickness	0.2 mm

[a]Modern Plastic *Encyclopedia*.[22]

Table 2 Properties of piezoelectric actuator

Composition	PSI-5A-S4-ENH[a]
Piezoelectric strain coefficient, m/V, $d_{31} = d_{32}$	-190×10^{-12}
C/s dimension, mm, $b \times t$	23.8×0.267
Modulus of elasticity, N/mm^2, $Y_1 = Y_2$	6.6×10^4

[a]Data available from URL: http://www.piezo.com [cited 20 Feb. 2002].

Change in path length $p(x)$ as a result of this deflection is the sum of the differences in two path segments, that is,

$$p(x) = (FN' - FN) + (N'P - NP) \tag{3}$$

The phase difference $f(x)$ caused by the path difference is given by

$$f(x) = 2\pi[p(x)/\lambda] \tag{4}$$

This $f(x)$ is used in Eq. (2) to calculate radiation intensity in various directions. The mesh used for numerical integration of Eq. (2) is the same as in finite element model (1050×3 elements). A large number of elements are taken along aperture length so that each element is of the size of $\frac{1}{3}$ of the wavelength of the antenna. Such a small size is needed for proper integration of radiation intensity function. The component of deflection at the middle of the antenna width and perpendicular to the aperture is used for the purpose of calculation of the radiation pattern.

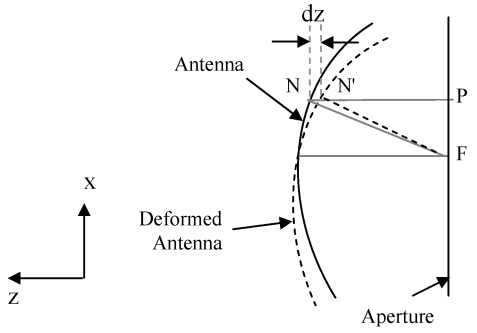

Fig. 12 Radiation pattern calculation.

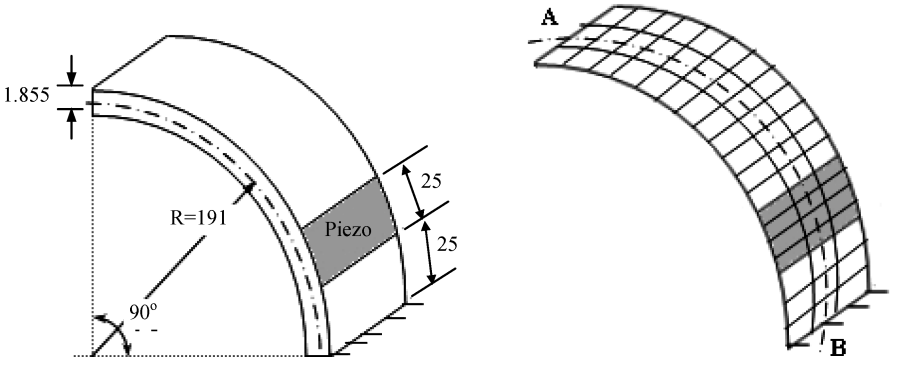

a) Dimensions **b) Typical mesh**

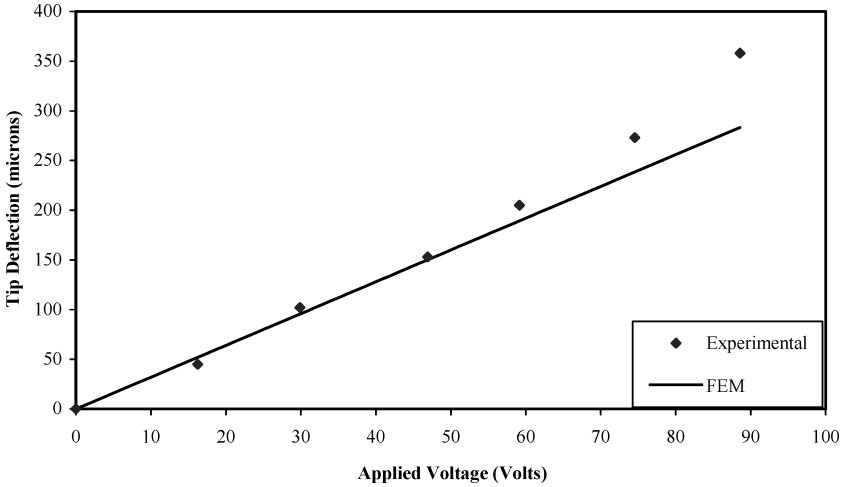

c) Variation of deflection with voltage for circular curved beam

Fig. 11 Circular curved-beam experiments (modulus of elasticity $Y_s = 0.638 \times 10^5$ N/mm^2 and cross section 25.9×1.855 mm for curved-beam; refer to Table 2 for piezoelectric actuator properties).

IV. Steering the Radiation Pattern

For steering of the radiation pattern, the apex of the parabola is fixed, and actuators are placed symmetrically on either side of the center. The two actuators are given opposite fields to obtain a skew-symmetric phase variation. The aim is to obtain a near-linear phase variation.

A. Effect of Pair of Central Actuators

Figure 13a shows the deflection induced by two actuators of 50 mm length, each placed on either side of the center with applied voltages of 300 and −300 V, respectively. Figure 13c shows the corresponding radiation pattern.

The peak intensity occurs at 4.62 deg, but many lobes of high intensity are observed. When actuator lengths are varied, similar patterns are obtained. The number of side lobes increases when the actuator length increases, as the nonlinear portion of deflection increases. The radiation field intensity plotted in the figure is normalized with the peak intensity of the undeformed antenna.

B. Improving the Quality of Steered Radiated Pattern

To understand the adverse effect of the nonlinear portion of deflection, phase variation induced by two centrally placed actuators is plotted in Fig. 13b. The nonlinear portion at the center of the phase variation is caused by the nonlinear deflection. What is more important to note is that the remaining portion where deflection is linear (see Fig. 13a) also has nonlinear phase variation because of the nonlinearity of path difference p with respect to x.

Because a linear phase variation is better, additional actuators (C and D) of length 50 mm are mounted at a distance 50 mm from the end of first actuators (A and B, respectively) (Fig. 14), and when the additional actuators are supplied with an electric field of 100 V, the phase variation becomes almost linear (Fig. 15a). The corresponding radiation pattern is plotted in Fig. 15b. The number of side lobes is drastically reduced in this case, but still a side lobe of almost the same amplitude as the main lobe is obtained. The occurrence of two large peaks side by side is caused by phase lag between the linear portions in two halves (Fig. 15a) not being a multiple of 2π.

It is attempted to merge the two peaks obtained in case of 50-mm-length actuator by making the lag between the two antenna halves a multiple of 2π by adjusting the voltage applied to the actuators at the center of the antenna. When the voltage on actuators A and B is reduced from 300 to 215 V, phase lag becomes 3.97π radians (Fig. 15c), and the radiation pattern shown in Fig. 15d is obtained. Significant improvement in radiated beam quality is observed. Thus, appropriate placement of actuators and suitable adjustment of voltages give significant improvement in the radiated beam quality. In this case, because of the significant reduction in voltage supplied to the central pair of actuators the shift decreases to 3.26 deg from 4.62 deg, but the radiated beam quality (measured in terms of side-lobe ratio) has improved significantly (from 1.05 to 2.40).

C. Optimal Steering

It is now attempted to obtain maximum steering with optimal radiation pattern quality in terms of peak intensity and side-lobe ratio. Steering is achieved by using a pair of actuators at the center, with the two actuators on either side having the same length. When the lengths of the two central actuators are increased, the radiated beam is steered more. Radiation pattern quality is optimized by using off center actuators to "straighten out" phase variation along the length. Length of the off-center actuators and voltage supplied to them are determined by trial and error. First, different lengths are tried, to obtain a reasonably straight phase variation, and then voltage is adjusted to make it as straight as possible.

Four optimal radiation patterns obtained are shown in Fig. 16. As actuator length increases, the main lobe shifts more, but the radiation pattern quality deteriorates as the number of side lobes increases. It can be observed that the ratio of shift to HPBW is very high in this case (up to 42 for the 100-mm actuator), indicating that main lobe has been steered well out of the original area scanned by the antenna.

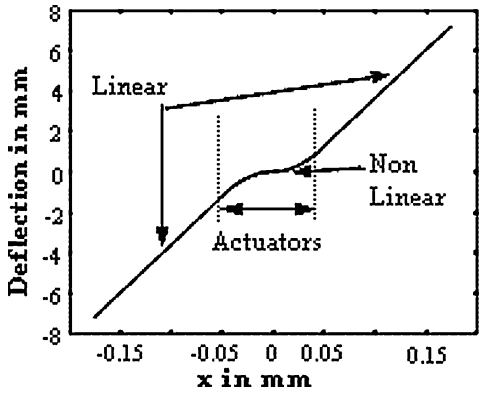

a) Induced deflection

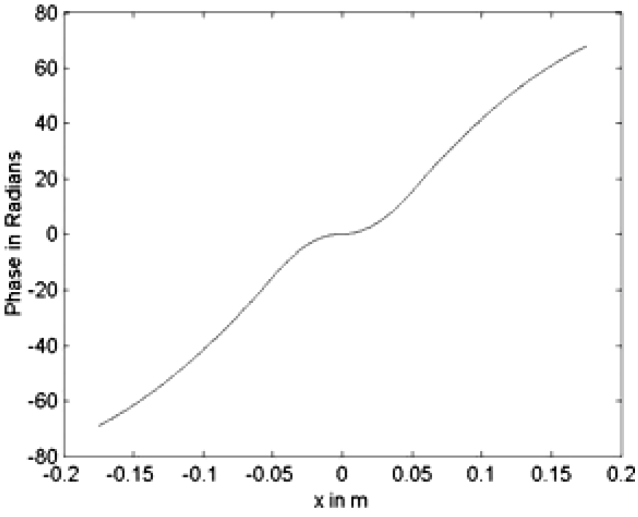

b) Phase pattern

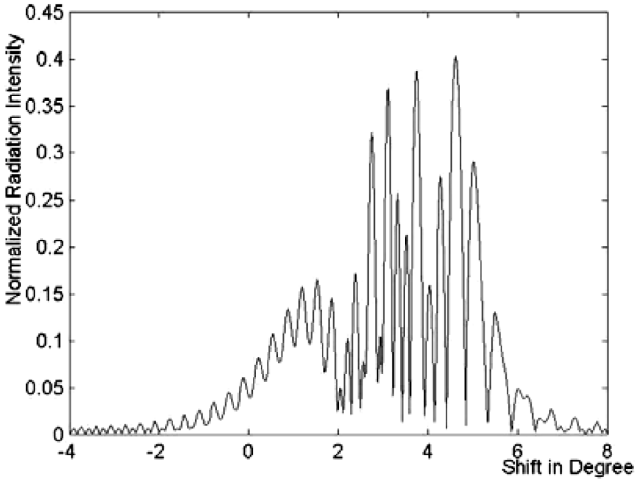

c) Radiation pattern

Fig. 13 Effect of 50-mm actuator on radiation pattern [wavelength = 1 mm, aperture length = 0.35 m, focal length f = 0.151 m, angle covered (2α) = 120 deg].

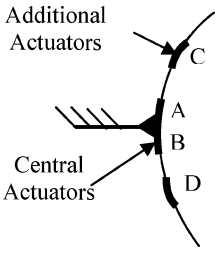

Fig. 14 Mounting of additional actuator.

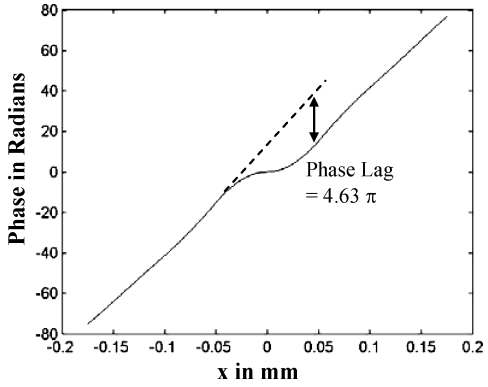

a) Phase pattern (for $V_A = V_B = 300$ V, $V_C = V_D = 100$ V)

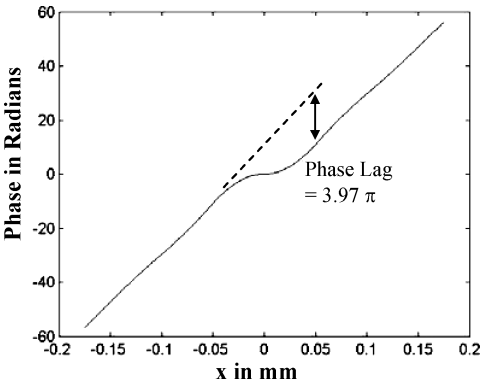

c) Phase pattern (for $V_A = V_B = 215$ V, $V_C = V_D = 100$ V)

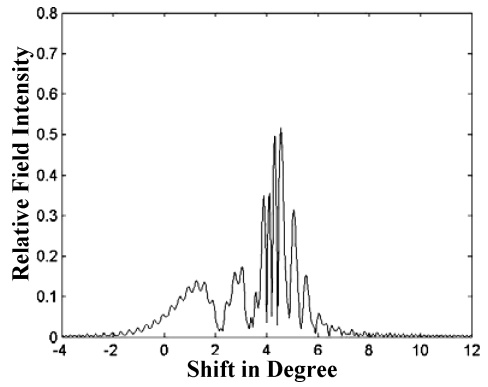

b) Radiation pattern (for $V_A = V_B = 300$ V, $V_C = V_D = 100$ V)

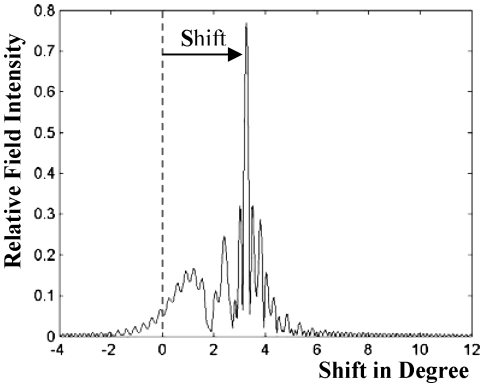

d) Radiation pattern (for $V_A = V_B = 215$ V, $V_C = V_D = 100$ V)

Fig. 15 Improving quality of steered radiated beam (50-mm actuator).

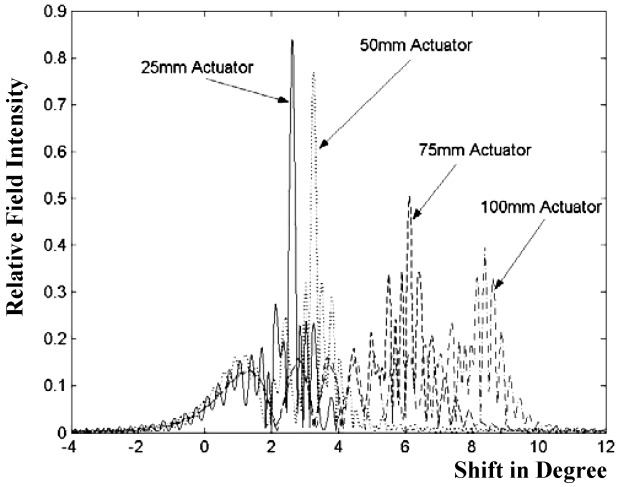

Fig. 16 Effect of center actuator length (A and B) on radiation pattern of cylindrical antenna [wavelength = 1 mm, aperture length = 0.35 m, focal length $f = 0.151$ m, angle covered $(2\alpha) = 120$ deg].

The variation of relative field intensity and side-lobe ratio with shift are plotted in Figs. 17a and 17b, respectively.

As the shift increases, both side-lobe ratio and relative field intensity decrease. Relative field intensity and side-lobe ratios are more correlated to shift than to voltage applied or actuator length. It indicates that optimal quality for a specific amount of steering can perhaps be achieved with different combinations of lengths and voltages.

The increase in side lobes and decrease in field intensity of main lobe with increase in actuator length appear to be caused by an increase in the nonlinear portion of phase variation at the center. Good results are obtained here on the basis of simple heuristics of making the phase variation linear and adjusting the phase lag. It will be possible to improve these results using optimization, but that is not attempted here.

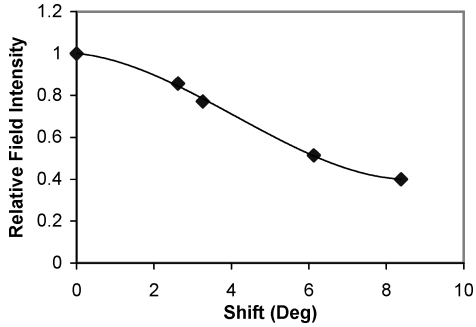

a) Variation of relative field intensity

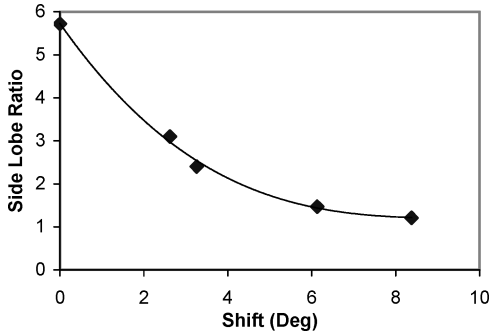

b) Variation of side-lobe ratio

Fig. 17 Variation of performance parameters with shift.

V. Optimal Shaping

In Sec. II.B, it was observed that a piecewise linear symmetric phase variation at aperture leads to two equal and separated lobes (Fig. 6). Here, it has been attempted to obtain two separated lobes with piezoactuation. This can be achieved by supplying voltage with the same polarity to the two actuators, whereas for steering the radiated beam the voltage was supplied in opposite directions.

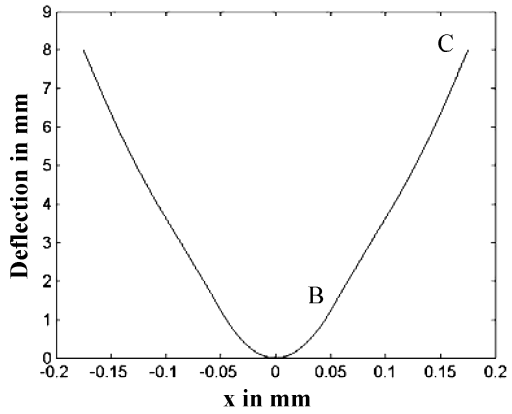

a) Deflection pattern (for 50-mm actuator at center and 50-mm additional actuator and $V_A = V_B = 300$ V, $V_C = V_D = 100$ V)

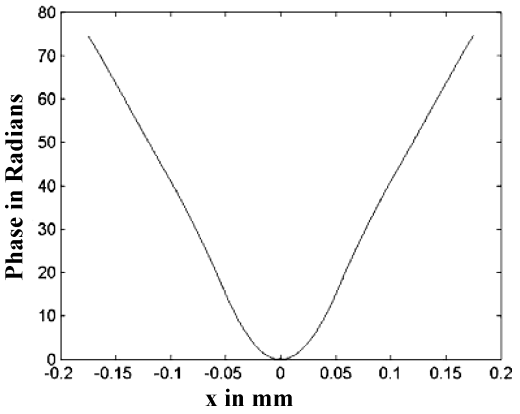

b) Corresponding phase plot (for 50-mm actuator at center and 50-mm additional actuator and $V_A = V_B = 300$ V, $V_C = V_D = 100$ V)

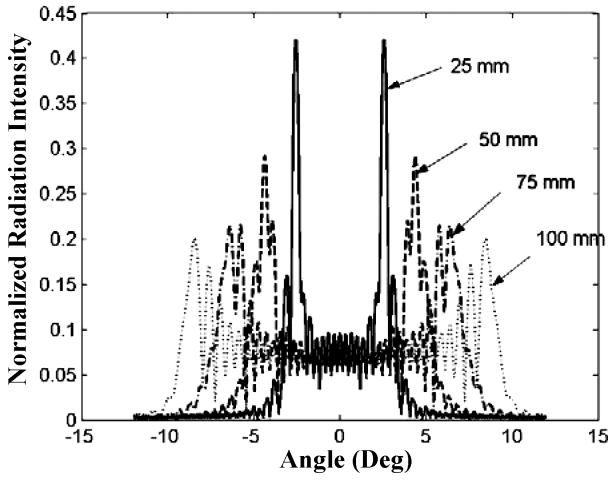

c) Radiation pattern

Fig. 18 Radiated beam shaping using piezoelectric actuator [wavelength = 1 mm, aperture length = 0.35 m, focal length $f = 0.151$ m, angle covered $(2\alpha) = 120$ deg].

Additional actuators are placed to straighten out the nonlinear phase variation.

Deflection induced as a result of piezoelectric actuation is shown in Fig. 18a for a 50-mm center actuator and an additional 50-mm actuator (discussed in Sec. IV.B). It can be seen in Fig. 18b that the additional actuator has straightened out the phase variation in the region BC. The corresponding radiation pattern is plotted in Fig. 18c. Pairs of distinct peaks can be observed located symmetrically on either side of $\theta = 0$.

With an increase in actuator length, the distance between the peaks increases, but the field intensity decreases. This occurs because of the increase in loss of focused energy in the middle portion. No phase lag adjustment is needed in this case. Variation of relative field intensity and side-lobe ratio with separation between peaks is plotted in Figs. 19a and 19b, respectively. As the separation increases, both side-lobe ratio and relative field intensity decrease. This appears to be caused by the increase in actuator length and consequent increase in the nonlinear portion of phase variation at the center.

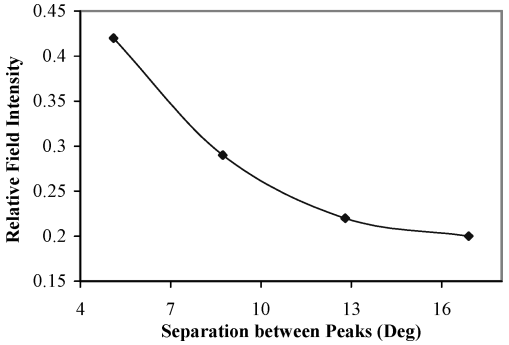

a) Variation of relative field intensity

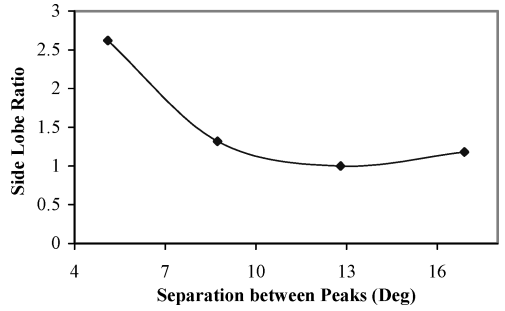

b) Variation of side-lobe ratio

Fig. 19 Variation of performance parameters with peak separation.

VI. Conclusions

In this paper, the changes in the radiation pattern of a parabolic cylindrical antenna, induced by piezoelectric actuators, have been analyzed and near-optimal steering and shaping obtained. For the chosen antenna and piezoelectric actuators, it is possible to shift the main lobe substantially, by about 5–10 deg [i.e., about 25–50 times the half-power beamwidth (HPBW)] for steering and obtain two main lobes separated by 10–20 deg (i.e., about 50–100 times the HPBW) for shaping. The manner of piezoactuation used here is motivated by the influence of linear phase variation of the aperture on radiation pattern. It has been shown that nonlinear phase variation can be made linear by appropriately adjusting the placement of actuators and the field applied. By adjusting the field applied to the actuators, the path difference between the linear portions of antenna deflections could be adjusted, leading to significant improvement in the quality of the steered radiation pattern.

Acknowledgment

The authors are thankful to the Department of Science and Technology, Government of India, for funding the research work.

References

[1]Agrawal, B. N., and Treanor, K. E., "Shape Control of a Beam Using Piezoelectric Actuators," *Smart Materials and Structures*, Vol. 8, No. 6, 1999, pp. 729–740.

[2]Agrawal, S. K., and Nagaraja, K., "Application of Piezoelectric Actuators for Shape Control of Elastic Plates," *Journal of Intelligent Material Systems and Structures*, Vol. 5, No. 4, 1994, pp. 514–522.

[3]Wang, C. M., Ang, K. K., and Ajit, A., "Shape Control of Laminated Cantilevered Beams with Piezoelectric Actuators," *Journal of Intelligent Material Systems and Structures*, Vol. 10, No. 2, 1999, pp. 164–175.

[4]Yang, S., and Ngoi, B., "Shape Control of Beams by Piezoelectric Actuators," *AIAA Journal*, Vol. 38, No. 12, 2000, pp. 2292–2298.

[5]Ghosh, K., and Batra, R. C., "Shape Control of Plates Using Piezoceramic Elements," *AIAA Journal*, Vol. 33, No. 7, 1995, pp. 1354–1357.

[6]Tong, D., WilliamsII, R., and Agarwal, S. K., "Optimal Shape Control of Composite Thin Plates with Piezoelectric Actuators," *Journal of Intelligent Material Systems and Structures*, Vol. 9, June 1998, pp. 458–467.

[7]Fukunaga, H., Sekine, H., and Matsuno, Y., "Static Deformation Control of a Laminated Composite Plate with Piezoelectric Actuators," *JSME International Journal Series A*, Vol. 41, No. 2, 1998, pp. 267–273.

[8]Chee, C. Y. K., Tong, L., and Steven, G. P., "A Review on the Modeling of Piezoelectric Sensors and Actuators Incorporated in Intelligent Structures," *Journal of Intelligent Material Systems and Structures*, Vol. 9, No. 1, 1998, pp. 3–18.

[9]Irschik, H., "A Review on Static and Dynamic Shape Control of Structures by Piezoelectric Actuation," *Engineering Structures*, Vol. 24, No. 1, 2002, pp. 5–11.

[10]Washington, G. N., "Smart Aperture Antennas," *Smart Materials and Structures*, Vol. 5, No. 6, 1996, pp. 801–805.

[11]Yoon, H. S., and Washington, G., "Piezoceramic Actuated Aperture Antennae," *Smart Materials and Structures*, Vol. 7, No. 4, 1998, pp. 537–542.

[12]Yoon, H. S., Washington, G., and Theunissen, W. H., "Analysis and Design of Doubly Curved Piezoelectric Strip-Actuated Aperture Antennas," *IEEE Transactions on Antennas and Propagation*, Vol. 48, No. 5, 2000, pp. 755–763.

[13]Kiely, E., Washington, G., and Bernhard, J., "Design and Development of Smart Microstrip Patch Antennas," *Smart Materials and Structures*, Vol. 7, 1998, pp. 792–800.

[14]Bhatti, A., and AL Raweshidy, H. S., "D-Fiber Antenna Characterization Using Finite Element Analysis," *IEEE Journal of Quantum Electronics*, Vol. 37, No. 8, 2001, pp. 970–979.

[15]Gupta, V. K., "Studies on Piezoelectric Actuated Shell with Application to Optimal Steering of Antenna," Ph.D. Dissertation, Mechanical Engineering Dept., Indian Inst. of Technology Bombay, Mumbai, India, July 2003.

[16]Stutzman, W. L., and Thiele, G. A., *Antenna: Theory and Design*, Wiley, New York, 1998.

[17]Balanis, C. A., *Antenna Theory: Analysis and Design*, 2nd ed., Wiley, New York, 1989, Chaps. 2 and 15.

[18]Ahmad, S., Irons, B. M., and Zienkiewicz, O. C., "Analysis of Thick and Thin Shell Structures by Curved Finite Elements," *International Journal for Numerical Methods in Engineering*, Vol. 2, No. 3, 1970, pp. 419–451.

[19]Gupta, V. K., Seshu, P., and Issac, K. K., "Finite Element and Experimental Investigation of Piezoelectric Actuated Smart Shells," *AIAA Journal*, Vol. 42, No. 10, 2004, pp. 2112–2123.

[20]Panda, S. C., and Natarajan, R., "Finite Element Analysis of Laminated Composite Plates," *International Journal of Numerical Methods in Engineering*, Vol. 14, No. 1, 1979, pp. 69–79.

[21]Panda, S. C., and Natarajan, R., "Analysis of Laminated Composite Shell Structure by Finite Element Method," *Computers and Structures*, Vol. 14, No. 3–4, 1981, pp. 225–230.

[22]Modern Plastics, *Encyclopedia 1990*, Vol. 66, No. 11, McGraw–Hill, New York, 1989, pp. 472–570.

M. Ahmadian
Associate Editor